

# A semiclassical analysis of the Efimov energy spectrum

Rajat K. Bhaduri,<sup>1</sup> Matthias Brack,<sup>2</sup> and M. V. N. Murthy<sup>3</sup>

<sup>1</sup>*Department of Physics and Astronomy,*

*McMaster University, Hamilton, Canada L9H 6T6*

<sup>2</sup>*Institute for Theoretical Physics, University of Regensburg, D-93040 Regensburg, Germany*

<sup>3</sup>*Institute of Mathematical Sciences, Chennai, 600 113 India*

(Dated: May 3, 2019)

## Abstract

We demonstrate that the ( $s$ -wave) geometric spectrum of the shallow Efimov energy levels is generated by the radial motion of a primitive periodic orbit of the corresponding classical system and its harmonics. The action of the primitive orbit is given by the logarithm of the energy. This is shown to be consistent with the leading term of an inverse-squared radial potential with a lower cut-off radius. The lowest-order WKB quantization, including the Langer correction, is shown to reproduce the geometric scaling of the energy spectrum. The (WKB) mean-squared radii of the Efimov states scale geometrically like the inverse of their energies. The WKB wavefunctions, regularized at the classical turning point using Langer's connection formula, are practically indistinguishable from the exact wave functions even for the lowest ( $n = 0$ ) state, apart from a tiny shift of its zeros that remains constant for large  $n$ .

## I. INTRODUCTION

Two particles that are just shy of binding may develop an infinite number of shallow bound states when a third particle is added. This was predicted by Efimov [1] forty years back, and has only been recently verified experimentally with an ultra-cold gas of optically trapped  $^{133}\text{Cs}$  atoms [2]. Subsequently, Barontini *et al.* [3] have found evidence for two kinds of Efimov trimers with  $^{41}\text{K}$  and  $^{87}\text{Rb}$  atoms. Efimov considered three identical bosons interacting pairwise with an interaction whose range  $r_0$  is much smaller than the interatomic scattering length  $a$ . Using the hyperspherical coordinates for the three-body problem, he showed that the effective potential in the hyperradial coordinate  $R$  between the length scales of  $r_0$  and  $|a|$  is of an inverse-squared type. In the symmetric  $L = 0$  three-body state, this effective interaction is sufficiently attractive to give rise to the Efimov spectrum for the trimers. A signature of the Efimov spectrum is its geometric scaling, with the ratio of the adjacent energy levels being constant. This was predicted by Efimov [1] and has been verified by recent experiments [4].

In Sec. II, we will discuss the geometric spectrum and interpret it semiclassically. In the periodic orbit theory (POT) [5], there is an intimate connection between classical periodic orbits and the quantum energy spectrum of a system through so-called trace formulae (cf. [6] for an introduction and applications of the POT). For an energy spectrum governed by only one quantum number, there is a rather simple way of deriving a trace formula. This will be done for the Efimov spectrum in Sec. II, where we also show that the action of the periodic orbit generating the quantum spectrum depends logarithmically on the energy.

In Sec. III, we first derive the quantum-mechanical solutions of the inverse-squared potential with a lower cut-off radius  $R_c$ . The exact quantum wave function is a modified Bessel function of imaginary order [7]. Next we derive the leading-order WKB wave function (including the Langer correction [8]). We show that its leading term in the classically allowed region is identical with the leading term of the exact wave function for high-lying states ( $n \gg 1$ ), responsible for the geometric scaling of the spectrum. In the classically forbidden region, it decays exponentially like the exact one. The WKB eigenvalues are obtained by quantising the classical action of the inverse-squared potential, whose leading term is the action appearing in the semiclassical trace formula discussed in Sec. II. We find that the WKB spectrum, although slightly phase shifted with respect to the exact one, reproduces

the geometric scaling of the quantum-mechanical energies and mean-squared radii with the same scaling factor. Remarkably, the WKB wave functions, when regularized at the turning point with Langer's connection formula [8], are – apart from their slightly shifted zeros – practically indistinguishable from the quantum-mechanical wave functions even for the lowest state ( $n = 0$ ).

## II. GEOMETRIC SPECTRUM

Efimov [1] showed that for three identical bosons in the symmetric  $s$  state ( $L = 0$ ), the energy spectrum obeys geometric scaling

$$E_n = E_0 \exp(-2\pi n/s_0), \quad n = 0, 1, 2, \dots \quad (1)$$

so that  $E_{n+1}/E_n$  is constant and independent of  $n$ .  $E_0 < 0$  and  $s_0 > 0$  are constants that depend on the system. For three equal-mass bosons, one has

$$\exp(\pi/s_0) = 22.694, \quad \Rightarrow \quad s_0 = 1.00624. \quad (2)$$

The energy  $E_0$ , which corresponds to the lowest quantum state of the system ( $n = 0$ ), introduces a length scale whose origin will be made clear soon. Our objective here is to derive an exact semiclassical trace formula for the density of states corresponding to the spectrum given by Eq. (1). This will enable us to identify the action of a single periodic orbit that generates the above spectrum. Following [6] (Chapter 3.2.2), we write  $E_n = f(n)$ , with degeneracy  $D(n) = 1$ . The function  $f(n)$  is monotonic with a differentiable inverse,  $f^{-1}(x) = F(x)$ . The exact density of states, defined by

$$g(E) = \sum_n \delta(E - E_n), \quad (3)$$

can then be rewritten, using Poisson resummation, as

$$g(E) = |F'(E)| \sum_{n=0}^{\infty} \delta(n - F(E)) = |F'(E)| [1 + 2 \sum_{k=1}^{\infty} \cos(2\pi k F(E))]. \quad (4)$$

This result, which is exact, can be split into two parts: a Thomas-Fermi term  $\tilde{g}(E) = |F'(E)|$  which gives its average behaviour, and an oscillating term which we denote by  $\delta g(E)$ .

In the semiclassical POT [5], the oscillating part of the exact density of states of a quantum Hamiltonian is expressed as a sum over the periodic orbits of the corresponding

classical Hamiltonian:

$$\delta g(E) = \sum_{\Gamma} \sum_{k=1}^{\infty} \mathcal{A}_{\Gamma,k} \cos \left[ \frac{k}{\hbar} S_{\Gamma}(E) - \sigma_{\Gamma,k} \frac{\pi}{2} \right] \quad (5)$$

The sum is over primitive periodic orbits ( $k = 1$ ), denoted by  $\Gamma$ , and their repetitions (harmonics)  $k > 1$ . The amplitude  $\mathcal{A}_{\Gamma,k}$  of a periodic orbit (assumed here to be isolated in phase space) depends on its primitive period and on its stability matrix. The phase factor  $\sigma_{\Gamma,k}$  is called the Maslov index of the periodic orbit. Comparing the simple trace formula (4) with the general form (5), we see that it has only one primitive periodic orbit  $\Gamma$  with action  $S(E) = 2\pi\hbar F(E)$ , and an amplitude  $2F'(E)$  which is proportional to its period. The Maslov index is zero. Since the spectrum is for  $s$  states only, the action is that of the *radial motion* in a central potential. For the geometric spectrum, inverting (1), we have

$$n(E) = \frac{s_0}{2\pi} \ln(E_0/E) = F(E). \quad (6)$$

Therefore the action  $S(E)$  of the primitive orbit is given by

$$S(E) = \hbar s_0 \ln(E_0/E). \quad (7)$$

Substituting  $F(E)$  in Eq. (4), we obtain

$$g(E) = \frac{s_0}{2\pi|E|} \left\{ 1 + 2 \sum_{k=1}^{\infty} \cos[k s_0 \ln(E_0/E)] \right\}. \quad (8)$$

This is an exact trace formula, representing a Fourier decomposition of (3). When summed over all harmonics, it reproduces the quantized spectrum (1).

The smooth part of the density of states  $\tilde{g}(E)$  is given by the first term on the r.h.s. of (8). The total number of Efimov states between the energies  $-|E_0|$  and  $-|E|$  is given by its integration over this interval, which yields Eq. (6).

Efimov trimers are formed when the two-body scattering length  $|a| \gg r_0$ , where the latter is of the order of the range of the intermolecular potential. One may then take the shallowest state to be  $E_a \simeq \hbar^2/ma^2$ , and the deepest state to have energy  $E_0 \simeq \hbar^2/mr_0^2$ . As  $a \rightarrow \pm\infty$ , there is an accumulation of states near zero energy. Substituting these in (6), we find the total number of Efimov states to be

$$N = \frac{s_0}{\pi} \ln(|a|/r_0). \quad (9)$$

The same result was obtained by Efimov following a different route. The above semiclassical analysis of the geometric spectrum of the Efimov states will now be put in the framework of a model Hamiltonian with an inverse-squared potential.

### III. THE INVERSE-SQUARED POTENTIAL

The three-body problem, after eliminating the center-of-mass coordinates, contains six degrees of freedom. In the hyperspherical formalism, these are described by a hyperradius

$$R = \sqrt{(r_{12}^2 + r_{23}^2 + r_{31}^2)/3} \quad (10)$$

and five hyperangular coordinates [9]. In the adiabatic approximation, for fixed  $R$ , the Schrödinger equation for the angular coordinates is solved to obtain a complete set of adiabatic eigenstates and the corresponding eigenvalues  $\epsilon(R)$ . In the resonant limit  $a \rightarrow \pm\infty$ , the angular variables decouple and one gets an effective inverse-squared potential in the coordinate  $R$ . The uncoupled hyperradial wavefunction in the  $L = 0$  state is  $\Psi(R) = R^{-5/2}u(R)$ . The reduced wavefunction  $u(R)$  obeys the Schrödinger equation (cf. [10])

$$\left[ -\frac{d^2}{dR^2} - \frac{(s_0^2 + 1/4)}{R^2} \right] u(R) = \frac{2mE}{\hbar^2} u(R), \quad (11)$$

where  $m$  is the mass of the atom and  $s_0$  the constant given in (2). In order to regularize the inverse-squared potential

$$V_0(R) = -\frac{\hbar^2}{2m} \frac{(s_0^2 + 1/4)}{R^2}, \quad (12)$$

we introduce a lower cut-off radius  $R_c \simeq r_0$  as shown schematically in Fig. 1.

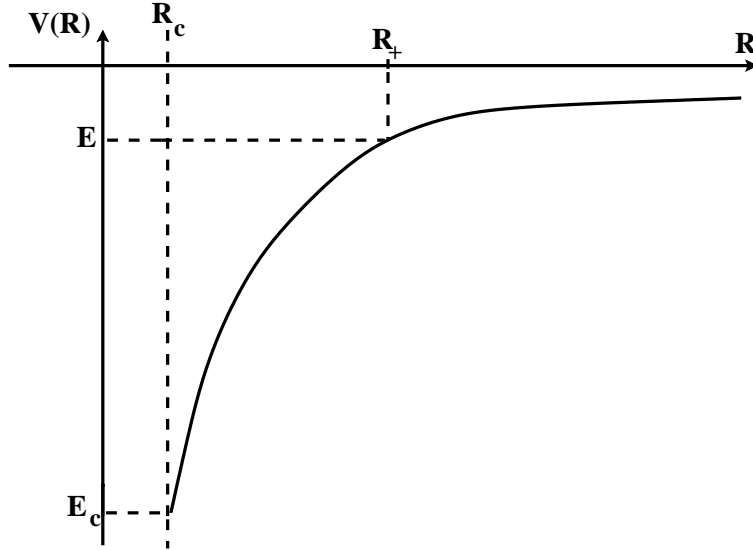


FIG. 1: A schematic of the inverse-square potential is shown.  $R_c$  is the cut-off radius;  $R_+$  denotes the outer classical turning point which is determined by the energy through  $E = V(R_+)$ .

For future convenience we introduce a dimensionless scaled variable  $x$  by

$$x = R/R_+, \quad x_c = R_c/R_+, \quad (13)$$

where  $R_+$  is the classical turning point at the energy  $E$

$$E = V(R_+) = -\hbar^2 s_0^2 / 2mR_+^2, \quad (14)$$

(see Sec. III B below), and the lowest energy  $E_c$  of the classical particle is given by

$$E_c = V(R_c) = -\hbar^2 s_0^2 / 2mR_c^2, \quad (15)$$

so that

$$x_c^2 = E/E_c. \quad (16)$$

### A. Quantum-mechanical solutions

We now solve the Schrödinger equation (11) with the lower boundary condition  $u(R_c) = 0$ . The second boundary condition comes from the requirement that the wave functions vanish at infinity. We introduce the following transformation

$$u(R) = \sqrt{R} w(R) \quad (17)$$

and obtain the equation for the function  $w(R)$  as

$$\frac{d^2 w}{dR^2} + \frac{1}{R} \frac{dw}{dR} + \frac{s_0^2}{R^2} w = -\frac{2mE}{\hbar^2} w. \quad (18)$$

Using the scaled variable  $x = R/R_+ = R\sqrt{-2mE/\hbar^2 s_0^2}$ , the above equation reduces to the standard form for the modified Bessel function

$$\frac{d^2 w}{dx^2} + \frac{1}{x} \frac{dw}{dx} - \frac{(is_0)^2}{x^2} w = w. \quad (19)$$

Thus, the energy scales away, which is a unique feature of the inverse-squared potential whose  $R$  dependence is the same as that of the kinetic energy operator. The solution to the equation (19) is given by a modified Bessel function with imaginary index  $is_0$

$$w(x) = K_{is_0}(y), \quad y = s_0 x, \quad (20)$$

which for real  $y$  and  $s_0$  is a real function that vanishes exponentially as  $y \rightarrow \infty$ . The eigenstates are found from its zeros as explained below.

To compute the function  $K_{i\nu}(y)$ , we use a power series expansion given in [11]:

$$K_{i\nu}(y) = -\sqrt{\frac{\nu\pi}{\sinh(\nu\pi)}} \sum_{k=0}^{\infty} \frac{(y^2/4)^k \sin[\nu \ln(y/2) - \phi_{\nu,k}]}{k! \nu \sqrt{\nu^2 + 1} \cdots \sqrt{\nu^2 + k^2}}, \quad (21)$$

where the phase  $\phi_{\nu,k}$  is given by

$$\phi_{\nu,k} = \arg \Gamma(1 + k + i\nu) = \phi_{\nu,0} + \sum_{s=1}^k \arctan\left(\frac{\nu}{s}\right). \quad (22)$$

$\phi_{\nu,0}$  and a convergent series for its calculation [12] are given by

$$\phi_{\nu,0} = \arg \Gamma(1 + i\nu) = -\nu \gamma + \sum_{s=0}^{\infty} \left( \frac{\nu}{1+s} - \arctan \frac{\nu}{1+s} \right), \quad (23)$$

where  $\gamma = 0.577215664 \dots$  is Euler's constant. Numerically we find

$$\phi_{s_0,0} = -0.30103393 \dots \quad (24)$$

As stated in [11], the function  $K_{i\nu}(y)$  has an infinite sequence of non-degenerate zeros  $y_n$  ( $n = 1, 2, \dots$ ) with  $0 < \dots < y_{n+1} < y_n < y_{n-1} \dots < y_1 < \nu$ , and no zeros for  $y \geq \nu$ . The solution to the Schrödinger equation (11) is therefore given by

$$u(x) = C \sqrt{y} K_{is_0}(y), \quad (y = s_0 x) \quad (25)$$

where  $C$  is a normalisation factor. The eigenspectrum is obtained from the zeros  $y_n$  via the boundary condition  $K_{i\nu}(y_n) = 0$  ( $n = 1, 2, \dots$ ).

It is an important feature of this system [13] that all eigenfunctions  $u_n(x)$  are given in terms of the universal solution (25) simply by letting the variable  $y$  in (25) start at the  $(n+1)$ st zero  $y_{n+1}$ . Fig. 2 shows this universal function in a doubly logarithmic plot, exhibiting the first 20 zeros. For  $x > 1$ , i.e.  $\ln(x) > 0$ , we notice the beginning of the exponential tail.

We can now associate the zeros with eigenvalues of the scaled cut-off  $x_c$  and write the eigenfunctions as

$$u_n(x) = C_n \sqrt{s_0 x} K_{is_0}(s_0 x), \quad x \geq (x_c)_n = y_{n+1}/s_0, \quad n = 0, 1, \dots \quad (26)$$

where  $C_n$  is the normalization constant of the  $n$ -th state. Note that  $n$  here is the number of zeros  $x_{n,j} > (x_c)_n$  ( $j = 0, 1, \dots, n$ ) of the functions  $u_n(x)$ . We found numerically that the  $C_n$  are practically identical for all  $n \geq 2$  (see Tab. I below), which is due to the fact that all

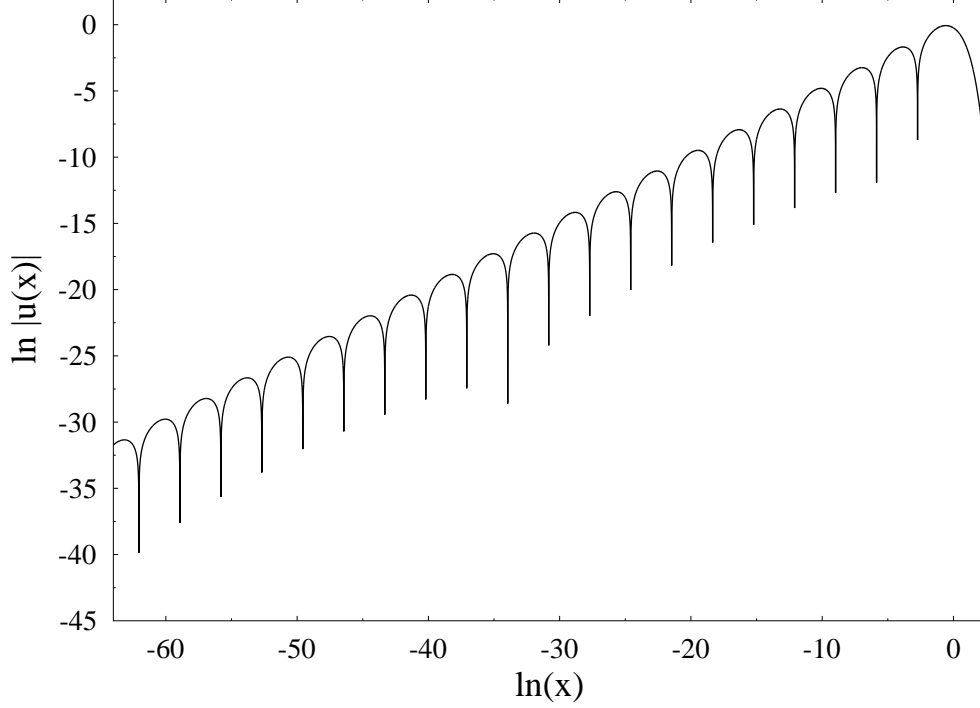


FIG. 2: The universal function  $u(x)$  in a doubly logarithmic plot. We see the first 20 zeros as negative spikes for  $\ln(x) < 0$ .

wave functions are peaked around  $x = 1$  and the regions below the first three zeros,  $y < y_3$ , give only exponentially small contributions to the norms.

In the region of the maximum of  $u(x)$  and the exponential tail for  $y \gtrsim 1$ , we had to include contributions to the sum in (21) up to  $k_{max} \gtrsim 25$ . For  $y \gtrsim 11$ , we did not, in fact, obtain convergence of the  $k$  sum. However, we found numerically that the leading term of an asymptotic form of  $K_{is_0}(y)$  for large  $y$ , given in [11]

$$u_n(x) \sim C_n \sqrt{\pi/2} \exp(-y), \quad (y \gg 1) \quad (27)$$

becomes sufficiently accurate for  $y \gtrsim 9$ .

For  $y \lesssim 0.3$ , the terms with  $k > 0$  of the series in (21) become numerically insignificant. Since the largest zero is found at  $y_1 = 0.0653423$  [cf.  $\ln(x_c)_0 = -2.73434$  in Tab. I below], this means that all zeros of  $K_{i\nu}(y)$  are given by the leading term with  $k = 0$ , yielding the asymptotic solution given in [9]

$$K_{i\nu}(y) \propto \sqrt{y} \sin[\nu \ln(y/2) - \phi_{\nu,0}]. \quad (n \gg 1) \quad (28)$$



Its zeros give the geometrical spectrum

$$E_n/E_c = (x_c)_n^2 \sim \left(\frac{2}{s_0}\right)^2 \exp(-2\pi n/s_0 - 2\pi/s_0 + 2\phi_{s_0,0}) \quad (n \gg 1) \quad (29)$$

which, apart from constants, is the same as that discussed in Sec. II; in particular, the constant ratio  $E_{n+1}/E_n$  remains the same. From (29) we get

$$\ln(x_c)_n \sim -n\pi/s_0 + \alpha_0, \quad (n \gg 1) \quad (30)$$

where  $\alpha_0$  is, using the actual constants in (2) and (24), given by

$$\alpha_0 = -\pi/s_0 + \phi_{s_0,0}/s_0 + \ln(2/s_0) = -2.73434. \quad (31)$$

In column 1 of Tab. I, we give some selected eigenvalues  $\ln(x_c)_n$  obtained numerically from the exact solutions above. Although the expression (30) is mathematically correct only asymptotically for large  $n$ , we find that the exact numerical eigenvalues agree with the r.h.s. of (30) and (31) within five digits – which corresponds to our numerical accuracy – even for  $n = 0$ .

$n$	$\ln(x_c)_n$ (QM)	$\ln(x_c)_n$ (WKB)	$\delta \ln(x_c)_n$	$1/C_n$
0	-2.73434	-2.64717	0.08717	0.3649953
1	-5.85644	-5.77053	0.08591	0.3651889
2	-8.97854	-8.89263	0.08591	0.3651892
10	-33.95535	-33.86943	0.08592	0.3651892
11	-37.07745	-36.99154	0.08591	0.3651892
20	-65.17635	-65.09044	0.08591	0.3651892
63	-199.42668	-199.34078	0.08590	0.3651892
100	-314.94440	-314.85850	0.08590	0.3651892

TABLE I: Eigenvalues  $\ln(x_c)_n$  of some selected states, obtained numerically both quantum-mechanically (QM) and in the WKB approximation discussed in Sec. II B. Column 3 gives their differences, and column 4 shows the inverse normalization constants  $C_n$  in (26).

It is quite remarkable that, with the value  $s_0 \simeq 1$  given for the present system, the geometrical nature of the Efimov spectrum is preserved with a high numerical accuracy all the way down to  $n = 0$  in the inverse-squared potential. For appreciably larger values of  $s_0$  this would not be the case.

## B. WKB solutions

We now present our results using the WKB approximation. Since the WKB method is well known, we need not present it here and refer for details to the text book by Migdal [14], who also discusses explicitly the Langer correction for radially symmetric potentials [8].

In the scaled variable  $x$ , the classical orbits are bounded inside the classically allowed region  $x_c \leq x \leq 1$ . Applying the Langer correction with the potential (12), the effective classical potential becomes

$$V(R) = -\frac{\hbar^2}{2m} \frac{s_0^2}{R^2}. \quad (R \geq R_c) \quad (32)$$

The classical momentum then is

$$P(R) = \sqrt{2mE + \hbar^2 s_0^2 / R^2}, \quad (33)$$

which, in the scaled variable  $x$ , becomes

$$P(R) = \frac{p(x)}{R_+} = \frac{p_0}{x} \sqrt{1 - x^2}, \quad p_0 = \frac{\hbar s_0}{R_+}. \quad (x_c \leq x < 1) \quad (34)$$

The standard WKB wave function in the classically allowed region has the form

$$u_{in}^{\text{WKB}}(x) = \frac{A}{\sqrt{p(x)}} \cos \left[ \frac{1}{\hbar} S_{in}(x) - \frac{\pi}{4} \right], \quad (x_c \leq x < 1) \quad (35)$$

where  $S_{in}(x)$  is the action integral along the orbit from  $x$  to 1:

$$S_{in}(x) = \int_x^1 p(x) dx = \hbar s_0 \int_x^1 \frac{\sqrt{1 - x^2}}{x} dx. \quad (x_c \leq x < 1) \quad (36)$$

This integral can be found analytically [15] and becomes

$$S_{in}(x) = \hbar s_0 \left[ \ln \left( \frac{1}{x} \right) + \ln \left( 1 + \sqrt{1 - x^2} \right) - \sqrt{1 - x^2} \right]. \quad (x_c \leq x < 1) \quad (37)$$

The boundary condition that the wave function (35) vanishes at the lower turning point  $x = x_c$  leads, like in the quantum-mechanical case, to the quantization of the eigenenergies as shown below.

Outside the classically allowed region ( $x > 1$ ), the exponentially decaying WKB wave function has the form

$$u_{out}^{\text{WKB}}(x) = \frac{B}{\sqrt{\kappa(x)}} \exp \left[ -\frac{1}{\hbar} S_{out}(x) \right], \quad \kappa(x) = \frac{\hbar s_0}{x} \sqrt{x^2 - 1}, \quad (x > 1) \quad (38)$$

with the action  $S_{out}(x)$  given by

$$S_{out}(x) = \int_1^x \kappa(x) dx = \hbar s_0 \left[ \arctan \left( \frac{1}{\sqrt{x^2 - 1}} \right) + \sqrt{x^2 - 1} - \frac{\pi}{2} \right]. \quad (x > 1) \quad (39)$$

For large  $x \gg 1$ , the function (38) has – apart from the normalization – the same exponential tail as the exact function (27):

$$u_{out}^{WKB}(x) \sim \frac{B e^{\pi/2}}{\sqrt{s_0 \hbar}} \exp(-s_0 x). \quad (s_0 x \gg 1) \quad (40)$$

Equating the two asymptotic forms (27) and (40), we can determine the constant  $B$  as

$$B_n = C_n \sqrt{s_0 \hbar \pi / 2} e^{-\pi/2}, \quad (41)$$

so that both wave functions agree exactly in the asymptotic tail region for each state  $|n\rangle$ .

Since both WKB functions (35) and (38) diverge at the upper classical turning point  $x = 1$ , where  $p(1) = \kappa(1) = 0$ , one must regularize these functions. This is done in the standard way [8, 14] by a linear approximation to the potential  $V(R)$  in the neighborhood of  $R = R_+$  and matching the corresponding Airy function solution to the above WKB wave functions at some suitable distances on either side of  $x = 1$ . The requirement that the wavefunction be continuous and continuously differentiable at both matching points leads to the relation  $A_n = 2B_n$  for the normalization constants and the phase  $-\pi/4$  in (35).

We now have to fulfil the lower boundary condition at  $x = x_c$ :

$$u_{in}^{WKB}(x_c) = 0 \quad \Rightarrow \quad \cos \left[ \frac{1}{2\hbar} S_0(E) - \frac{\pi}{4} \right] = 0, \quad (42)$$

where  $S_0(E)$  is the action of the primitive periodic orbit going from  $x_c$  to  $x = 1$  and back:

$$S_0(E) = 2 \int_{x_c}^1 p(x) dx, \quad (43)$$

which, using (37) and (16) becomes

$$S_0(E) = \hbar s_0 \left[ \ln(E_c/E) + 2 \ln \left( 1 + \sqrt{1 - E/E_c} \right) - 2\sqrt{1 - E/E_c} \right]. \quad (44)$$

For  $|E| \ll |E_c|$ , i.e. for the shallow states ( $n \gg 1$ ), the second and third terms above become negligible and the leading term reproduces the action (7) (with  $E_0 = E_c$ ) obtained from the periodic orbit theory applied to the geometric spectrum, as discussed in Sec. II. Eq. (42) has the solutions

$$\frac{1}{2\hbar} S_0(E) - \frac{\pi}{4} = \left( n + \frac{1}{2} \right) \pi, \quad n = 0, 1, 2, \dots \quad (45)$$

which yields the WKB quantization condition

$$S_0(E_n^{\text{WKB}}) = \oint P(R) dR = 2\pi\hbar(n + 3/4), \quad n = 0, 1, 2, \dots \quad (46)$$

Note that the constant  $3/4$  in (46) differs from the usual value  $1/2$ , which one obtains for smooth potentials, due to the hard-wall reflection at the lower turning point  $x_c$ .

Using only the asymptotically leading logarithmic term in (44) yields the geometric spectrum

$$E_n^{\text{WKB}} \sim E_c \exp[-2\pi/s_0(n + 4/3)], \quad (n \gg 1) \quad (47)$$

which corresponds to

$$\ln(x_c)_n \sim -n\pi/s_0 - 3\pi/4s_0 = -n\pi/s_0 - 2.34158. \quad (n \gg 1) \quad (48)$$

This is the same as the quantum-mechanical result (30), apart from a different shift (denoted by  $\alpha_0$  there). In column 2 of Tab. I, we give the WKB eigenvalues obtained from the quantization condition (46), using the full action (44), in terms of the scaled values  $\ln(x_c)_n$ . We see that they come very close to the exact quantum values. In fact, there remains a slight shift in  $\ln(x_c)_n$  that becomes constant for  $n \geq 1$  (cf. the third column in Tab. I). We interpret this shift as a higher-order semiclassical correction to the phase shift due to the cut-off radius  $R_c$ . Gibson [16] obtained an energy-independent phase shift from a  $\hbar$ -correction to the classical partition function of a finite box with a lower cut-off; unfortunately, we found no easy way to calculate it for the present potential (32).

We regularize the WKB functions (35), (38) using Langer's connection formula for one isolated classical turning point (Ref. [8], Eqs. (11a) and (11b) with  $\eta = 0$ ). Expressable in terms of a single Airy function  $\text{Ai}(\xi)$ , it reads

$$u_n^{\text{uni}}(x) = D_n \sqrt{\mathcal{S}(x)/|\xi|} \text{Ai}(\xi), \quad x \geq (x_c)_n \quad (49)$$

where  $D_n$  is a normalization constant, and

$$\xi = \left[ \frac{3}{2} \frac{1}{\hbar} S_{\text{out}}(x) \right]^{2/3}, \quad \mathcal{S}(x) = \frac{S_{\text{out}}(x)}{\hbar\kappa(x)} \quad \text{for } x \geq 1, \quad \xi \geq 0, \quad (50)$$

$$\xi = - \left[ \frac{3}{2} \frac{1}{\hbar} S_{\text{in}}(x) \right]^{2/3}, \quad \mathcal{S}(x) = \frac{S_{\text{in}}(x)}{\hbar p(x)} \quad \text{for } x \leq 1, \quad \xi \leq 0. \quad (51)$$

The superscript “uni” in (49) stands for “uniform”, because it turns out that (49) is a global uniform approximation that can be used not only in the vicinity of the classical turning

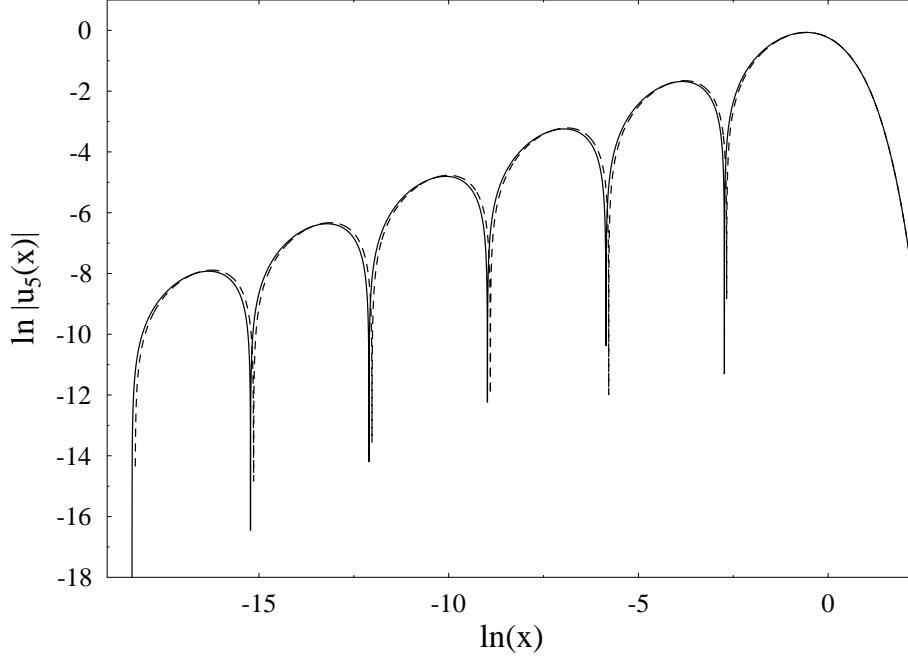


FIG. 3: The state  $u_5(x)$  in a doubly logarithmic plot. Solid line: exact normalized quantum-mechanical solution (26). Dashed line: normalized uniform WKB approximation (49).

point, but throughout the whole domain  $(x_c)_n \leq x < \infty$ . By construction [8], it yields the asymptotic WKB solutions (35), (38) sufficiently far from the turning point  $x = 1$ .

The normalized uniform WKB wavefunction (49) for  $n = 5$  is shown in Fig. 3, along with the exact one, in a doubly logarithmic plot. Apart from the slightly shifted zeros, there is a surprisingly good agreement. Fig. 4 shows the ground-state wave function for  $n = 0$ , both exactly (solid line), the “raw” WBK approximation (dotted line), and in the uniform approximation (49) (dashed line). Even for this lowest state, the quantum-mechanical and the uniform WKB solutions are practically indistinguishable.

### C. Mean squared radii

The size of our system in the  $n$ -th state is given by the mean squared hyperradius defined as

$$\langle R^2 \rangle = \frac{\langle \Psi_n | R^2 | \Psi_n \rangle}{\langle \Psi_n | \Psi_n \rangle} = R_+^2(E_n) \int_{x_c}^1 dx x^2 |u_n(x)|^2, \quad (52)$$

where Eq. (13) and the normalized wavefunctions  $u_n(x)$  have been used. Since  $R_+^2$  scales like  $1/E_n$ , see (14), the ratio of mean squared radii of two successive states is  $E_n/E_{n+1}$ , if the expectation values  $\langle n | x^2 | n \rangle$  remain independent of  $n$ .

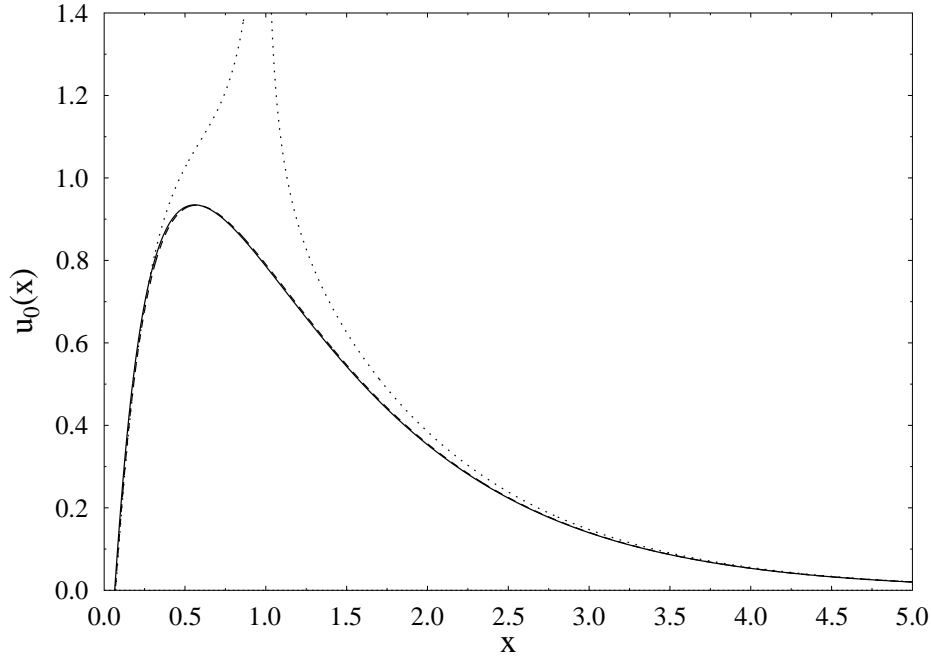


FIG. 4: The ground state  $u_0(x)$  in a linear plot. Solid line: exact normalized quantum-mechanical solution (26). Dotted line: WKB approximation (35), (38), normalized to the exact solution in the tail region via equation (41). Dashed line: normalized uniform WKB approximation (49).

That this is, indeed, the case for all  $n \geq 1$ , is demonstrated in Tab. II, both for the quantum-mechanical and the uniform WKB solutions. Thus the mean squared radius increases by the same geometric scaling factor as the energy decreases, as discussed in [9], also in the WKB approximation.

$n$	$\langle n x^2 n\rangle$ (QM)	$\langle n x^2 n\rangle$ (WKB)
0	1.3265	1.3408
1	1.3251	1.3392
2	1.3251	1.3392
5	1.3251	1.3392
10	1.3251	1.3392

TABLE II: Mean squared radii  $\langle n|x^2|n\rangle$  of some states, obtained quantum-mechanically (QM) and in the uniform WKB approximation.

#### IV. SUMMARY

To summarise, we have shown that the ( $s$ -wave) geometric spectrum of the Efimov energy levels is semiclassically generated by a single periodic orbit whose action depends logarithmically on the energy. We first recapitulate the quantum spectrum of the inverse-squared potential with a lower cut-off and show, for  $s_0 \simeq 1$ , that it reproduces the geometric Efimov spectrum not only for shallow states, but yields the same constant ratio  $E_{n+1}/E_n$  all the way down to the ground state with  $n = 0$ . We have given an analytical expression for the zeros of the eigenfunctions. The WKB quantization of the classical system (including the Langer correction) yields the same spectrum, although slightly phase shifted, which preserves the same constant ratio  $E_{n+1}/E_n$  down to  $n = 0$ . The action of the classical system has as its leading term precisely the action obtained from the periodic orbit theory. The WKB wave functions, when regularized around the classical turning point using Langer's connection formula, reproduce the exact ones surprisingly well, apart from the slightly shifted zeros – even for the ground state ( $n = 0$ ). Both the quantum and the WKB solutions reproduce the geometric scaling of the mean squared radii of the Efimov states which is inverse to that of their eigenenergies.

R.K.B. and M.B. are grateful to the IMSc, Chennai, for its hospitality and excellent working conditions.

- 
- [1] V. Efimov, Phys. Lett. B **33**, 563 (1970); Sov. J. Nucl. Phys. **12**, 589.
- [2] T. Kraemer *et al.*, Nature **440**, 315 (2006).
- [3] G. Barontini *et al.*, Phys. Rev. Lett. **103**, 043201 (2009).
- [4] M. Zaccanti *et al.*, Nature Phys. **5**, 586 (2009);  
N. Gross *et al.* Phys. Rev. Lett. **103**, 163202 (2009);  
S. E. Pollack, D. Dries, and R. G. Hulet, Science **326**, 1683 (2009).
- [5] M. C. Gutzwiller, J. Math. Phys. **12**, 343 (1971);  
R. Balian and C. Bloch, Ann. Phys. (N.Y.) **69**, 76 (1972);  
M. V. Berry and M. Tabor, Proc. R. Soc. Lond. A **349**, 101 (1976).
- [6] M. Brack and R. K. Bhaduri: *Semiclassical Physics* (Bolder, Westview Press, 2003).
- [7] K. S. Gupta and S. G. Rajeev, Phys. Rev. D **48**, 5940 (1993).
- [8] R. E. Langer, Phys. Rev. **51**, 669 (1937).
- [9] E. Braaten and H-W. Hammer, Phys. Rep. **428**, 259 (2006).
- [10] For a pedagogical review, see R. K. Bhaduri, A. Chatterjee, and B. P. van Zyl, arXiv:quant-ph/1009.2713v2 (2010); Am. J. Phys., in print.
- [11] T. M. Dunster, SIAM J. Math. Anal. **21**, 995 (1990).
- [12] M. Abramowitz and I. A. Stegun: *Handbook of Mathematical Functions*, 9th printing (New York, Dover, 1972).
- [13] A. M. Essin and D. G. Griffiths, Am. J. Phys. **74**, 109 (2006).
- [14] A. B. Migdal: *Qualitative methods in quantum theory* (Reading, Benjamin, 1977)
- [15] I. S. Gradshteyn and I. M. Ryzhik: *Table of Integrals, Series, and Products* (New York, Academic Press, 5th edition, 1994).
- [16] W. G. Gibson, Phys. Rev. A **2**, 996 (1970).